Journal of Marine Science and Technology

Volume 25 | Issue 6 Article 5

THE NONLINEAR DYNAMICS AND ANTI-SWAY TRACKING CONTROL FOR OFFSHORE CONTAINER CRANE ON A MOBILE HARBOR

You-Gang Sun
Logistics Engineering College, Shanghai Maritime University, Haigang Ave, Shanghai, P.R. China. School of Mechanical Engineering, Tongji University, China., ygsun@shmtu.edu.cn

Hai-Yan Qiang
Logistics Engineering College, Shanghai Maritime University, Haigang Ave, Shanghai, P.R. China. School of Mechanical Engineering, Tongji University, China.

Junqi Xu
School of Mechanical Engineering, Tongji University, China.

Da-Shan Dong
Logistics Engineering College, Shanghai Maritime University, Haigang Ave, Shanghai, P.R. China.

THE NONLINEAR DYNAMICS AND ANTI-SWAY TRACKING CONTROL FOR OFFSHORE CONTAINER CRANE ON A MOBILE HARBOR

Acknowledgements

This research was supported by the National Natural Science Foundation of China (No. 51505277).

Journal of Marine Science and Technology, Vol. 25, No. 6, pp. 656-665 (2017)
DOI: 10.6119/JMST-017-1226-05

THE NONLINEAR DYNAMICS AND ANTI-SWAY TRACKING CONTROL FOR OFFSHORE CONTAINER CRANE ON A MOBILE HARBOR

You-Gang Sun[1, 2], Hai-Yan Qiang[1, 2], Junqi Xu[2], and Da-Shan Dong[1]

Key words: offshore container crane, nonlinear dynamics, ship motions, anti-sway control, position tracking.

ABSTRACT

The offshore container crane (OCC), as a novel maritime container transfer system, can handle container from a large container-ship anchored in open sea to address the congestion and limited water-depth of port. However, for the wave- and wind-induced movements of the ship, the crane's control system should be redesigned to ensure the load transfer on the sea. In this paper, we derive the nonlinear dynamic equations of OCC system subjected to the ship motions based on dynamic analysis. Then a double-layer sliding manifold is constructed to realize the position tracking and sway control simultaneously, irrespective of ship motions and parameters perturbation. The Lyapunov method is utilized to prove the stability of the proposed control law. Next, virtual prototype of the OCC is established, including the multi-body dynamics model of OCC with flexible rope and the proposed control scheme. Sufficient simulations are provided to illustrate its improved performance versus conventional controller. Experiments are also implemented to evaluate its practical control performance of trajectory following and sway angle suppression.

I. INTRODUCTION

With the integration of the global economy, rapid development has been made in container logistics industry. Meanwhile, the harbor congestion and modern large container-ship unable to dock at shallow waters harbor have become urgent problems (Oscar, 2015; Jin, 2016). Compared with the expansion of harbor scale, mobile harbors have become the most flexible, economical and environmental-friendly solution (Jonghoe, 2012; Baird, 2013). As illustrated in Fig. 1, this concept is to install

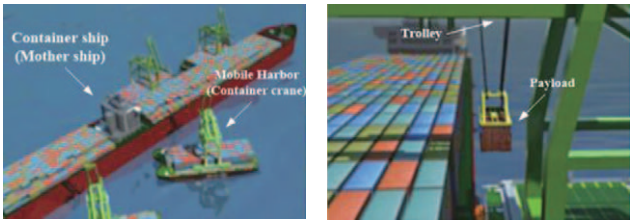

Fig. 1. The offshore container crane on mobile harbor.

ing the container crane on an offshore platform, which is called "offshore container crane" (OCC), to load and unload containers (payloads) for large container-ship anchoring in open sea and transport them to destination harbor (Jang, 2014).

Due to the effects of waves and trolley motion trajectory, the transferred payloads will generate a complex nonlinear dynamic response. Especially, the residual sway of payload decreases operation efficiency sharply, which can lead to serious damages. In fact, the trolley trajectory planning and payload anti-swing of land-based cranes are widely used in transportation and construction industries. There have also been a lot of research work focused on this area in the past two decades. The researchers in crane dynamics and control fields are interested in fast, no residual swing and high efficient anti-swing solutions. Existing work can be divided into open-loop control and closed-loop control. The open-loop control method with representative of input shaping (Garrido, 2008) and optimal control (Terashima, 2007) has a strong dependence on the accuracy of system mathematical model. The closed-loop control methods are usually combined with intelligent control, such as H-2/H-infinity Control (Hilhorst, 2015), fuzzy control (Chang, 2007; Li, 2015; Wu, 2016), neural networks control (Saeidi, 2013), sliding mode control (Almutairi, 2009), etc. Moreover, the dynamics and control strategies of ship-mounted cranes, which are divided into boom crane (Chin, 2001; Skaare, 2006; Sanfilippo, 2016) and container crane (Park, 2012; Le, 2015), also have been studied. Henry et al. (2001) proposed a delayed feedback control law to suppress the oscillations of the load of boom cranes. Cha et al. (2010) and Ham et al. (2015) studied the multi-body dynamics of floating cranes. Ngo et al. (2012) developed a sliding model controller based on Lyapunov method to reduce the sway angle of the con-

Paper submitted 06/14/17; revised 08/21/17; accepted 11/02/17. Author for correspondence: You-Gang Sun (e-mail: ygsun@shmtu.edu.cn).
[1] Logistics Engineering College, Shanghai Maritime University, Haigang Ave, Shanghai, P.R. China.
[2] School of Mechanical Engineering, Tongji University, China.

tainer crane. Sun et al. (2015) presented a self-adaptive PID controller based on GA to control the floating crane. Ismail et al. (2015) constructed a LQR-based sliding surface to track the crane's desired trajectory in the presence of waves and winds. Although the dynamics analysis and control of cranes have made great progress, there are still few researches on the OCC. It is necessary to improve the nonlinear dynamic equations of the offshore crane under the coupling influence of ship motions and trolley motions during lifting on the sea. Moreover, the present control approaches generally linearize the nonlinear dynamic model at the equilibrium point or neglect some nonlinear term in the equations to design the controller. It is feasible for land cranes since the external disturbance is little and the system is hardly far away from the equilibrium point. While for the offshore crane, there are permanent external disturbances from the sea environment. The system is easy to be far away from the equilibrium point by the effect of the disturbances, thus the performances of controllers based on the linear control theory will decrease greatly and even cause accidents. Therefore, it is urgent to design a nonlinear controller according to the nonlinear dynamic model of the crane under the ocean environment, without any linear approximation to ensure the control performance under permanent external disturbances.

The ship of mobile harbor, on which the container crane is installed, is easy to be disturbed away from the designated position horizontally and vertically. A lot of dynamic positioning systems have been proposed based on the nonlinear control theories to control the horizontal movement of the ship (Do, 2002; Serrano, 2014). On the other hand, the heave compensation system is designed to deal with the vertical shifting of the ship (Kuchler, 2011; Woodacre, 2015). However not enough attention has been paid to the rolling motion of the ship. For container transfer operations, the rolling motion of the ship holds great significance for the trolley position tracking and payload anti-sway.

Thus, in this paper, we construct dynamics equations of OCC system, which reveals the influence of ship motion and trolley movement on payload dynamic behavior, considering the trolley motion, heave motion and roll motion of the ship. An anti-sway tracking control strategy of SOSM (second order sliding mode) is presented for sway suppression and trajectory tracking despite the ship motion disturbances. We not only prove the stability of the sliding surface at all layers theoretically, but also implement the simulations and experiments to evaluate its excellent control performance.

II. DYNAMICS DEVELOPMENT AND ANALYSIS

For OCC system, due to the pitch motion of the ship, the lateral swing will be generated. But thanks to the immobilization of trolley at the lateral direction, many mechanical anti-sway devices can be utilized to eliminate lateral sway (Hong, 2009; Wang, 2013). Thus, this paper will not discuss the lateral anti-sway, which means we can ignore the pitch motion.

The three coordinate systems are introduced to derive mathematical dynamic equations of OCC, as shown in Fig. 2. OX_0Y_0 is the inertial coordinate frame, which defines the direction from port to starboard as positive direction of X_0 axis. $O_sX_sY_s$ denotes the ship coordinate frame affixed to the center of the gravity of the hull. $O_tX_tY_t$ denotes the trolley coordinate frame attached to the trolley. M, m respectively represents the masses of the trolley and the payload (container). h denotes the height of crane gantry. x and y are the trolley position and the ship heave displacement in the inertial coordinate frame. $l(t)$ is the varying length of rope. θ is the sway angle of payload in the plane of trolley motion. f_x is the control force applied to the trolley.

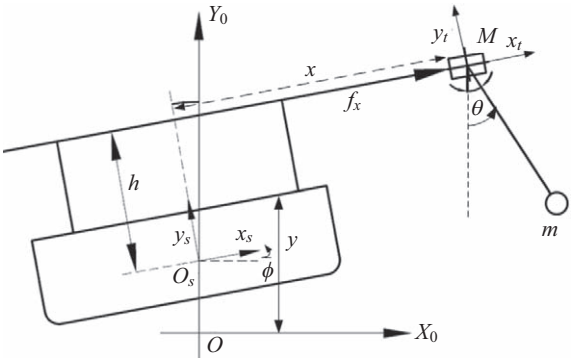

Fig. 2. Ship-crane-payload system and reference frames.

ϕ is roll angle of the ship under sea wave excitation. So ship motion vector is defined as (y, ϕ). In inertial coordinate frame, the trolley position p_M and payload position p_m can be derived as below:

$$p_M = \begin{bmatrix} x\cos\phi - h\sin\phi \\ y + h\cos\phi + x\sin\phi \end{bmatrix} \tag{1}$$

$$p_m = \begin{bmatrix} x\cos\phi - h\sin\phi + l\sin\theta \\ y + h\cos\phi + x\sin\phi - l\cos\theta \end{bmatrix} \tag{2}$$

Based on (1) and (2), trolley velocity v_M and payload velocity v_m can be obtained as follows:

$$v_M = \begin{bmatrix} v_{Mx} & v_{My} \end{bmatrix}^T \tag{3}$$

$$v_m = \begin{bmatrix} v_{mx} & v_{my} \end{bmatrix}^T \tag{4}$$

where

$$v_{Mx} = \dot{x}\cos\phi - x\dot{\phi}\sin\phi - h\dot{\phi}\cos\phi$$

$$v_{My} = \dot{y} + \dot{x}\sin\phi + x\dot{\phi}\cos\phi - h\dot{\phi}\sin\phi$$

$$v_{mx} = \dot{x}\cos\phi - x\dot{\phi}\sin\phi - h\dot{\phi}\cos\phi + \dot{l}\sin\theta + l\dot{\theta}\cos\theta$$

$$v_{my} = \dot{y} + \dot{x}\sin\phi + x\dot{\phi}\cos\phi - h\dot{\phi}\sin\phi - \dot{l}\cos\theta + l\dot{\theta}\sin\theta$$

The kinetic energy and potential energy of trolley-payload system are expressed as:

$$T = \frac{1}{2}M\left(v_{Mx}^2 + v_{My}^2\right) + \frac{1}{2}m\left(v_{mx}^2 + v_{my}^2\right) \tag{5}$$

$$\begin{aligned} U = {} & Mg(y + h\cos\theta + x\sin\phi) - m_p gl\cos\theta \\ & + m_p g\left(y + h\cos\phi + x\sin\phi\right) \end{aligned} \tag{6}$$

where, g denotes the acceleration of gravity. The ship's kinetic and potential energy are not included, since the ship motions (y, ϕ) are treated as external disturbance. $q = (x, \theta)$ is defined as generalized coordinate and $f = (f_x, 0)$ denotes generalized force. The Lagrange's equations are:

$$\frac{d}{dt}\left(\frac{\partial T}{\partial \dot{q}_i}\right) - \frac{\partial T}{\partial q_i} + \frac{\partial U}{\partial q_i} = f_i \tag{7}$$

The following nonlinear dynamic equations are obtained:

$$\begin{aligned} & (M+m)\ddot{x} - (M+m)x\dot{\phi}^2 - (M+m)h\ddot{\phi} + (M+m)\ddot{y}\sin\phi \\ & - ml\dot{\theta}^2\sin(\theta-\phi) + ml\ddot{\theta}\cos(\theta-\phi) + m\ddot{l}\sin(\theta-\phi) \\ & + (M+m)g\sin\phi + 2m\dot{l}\dot{\theta}\cos(\theta-\phi) = f_x \end{aligned} \tag{8}$$

$$\begin{aligned} & \ddot{x}\cos(\theta-\phi) + \ddot{y}\sin\theta + x\ddot{\phi}\sin(\theta-\phi) + l\ddot{\theta} + g\sin\theta \\ & - x\dot{\phi}^2\cos(\theta-\phi) - h\ddot{\phi}\cos(\theta-\phi) + 2\dot{l}\dot{\theta} \\ & - h\dot{\phi}^2\cos(\theta-\phi) + 2\dot{x}\dot{\phi}\sin(\theta-\phi) = 0 \end{aligned} \tag{9}$$

In order to verify the validity of dynamics model derived in Eqs. (8) and (9), an experimental setup is established. The specific parameters of the setup can be found in section V. A driving force $f_x = f_0 u(t)$ is applied to the trolley. $u(t)$ is step function once every 10 seconds. the amplitude f_0 is 10 N. The wave-induced rolling motion of the ship is set as $\phi(t) = 0.01\sin(0.8\,\text{time})$ rad. The Runge-Kutta method is utilized to obtain numerical solution for Eqs. (8) and (9) (Sun, 2017). The numerical results and experimental results, as shown in Figs. 3 and 4, are provided together for comparison. The results show that the numerical results of dynamics equations and the experimental results are basically consistent, which verify the validity of the derived dynamic equations.

III. CONTROL STRATEGY DESIGN AND ANALYSIS

A second order sliding mode (SOSM) position track and anti-sway control strategy is presented based on the nonlinear dynamics equations of OCC derived in the previous section.

Based on (8) and (9), the state space equations of OCC system can be obtained as follows:

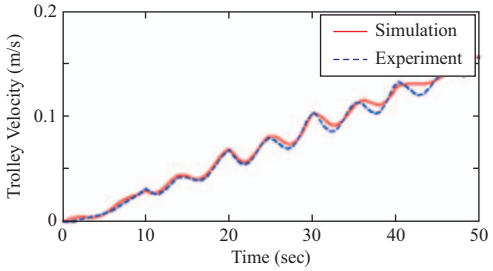

Fig. 3. The trolley velocity of theory and experiment.

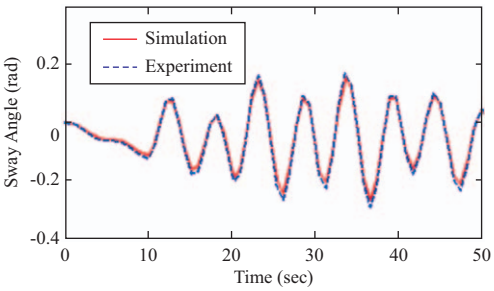

Fig. 4. The payload sway angle of theory and experiment.

$$\begin{cases} \dot{x}_1(t) = x_2(t), \\ \dot{x}_2(t) = g_1(X) + b_1(X)u + d_1(t), \\ \dot{x}_3(t) = x_4(t), \\ \dot{x}_3(t) = g_2(X) + b_2(X)u + d_2(t), \\ y(t) = [x_1(t), x_3(t)]^T \end{cases} \tag{10}$$

where, $x_1 = x, x_2 = \dot{x}, x_3 = \theta, x_4 = \dot{\theta}$, $u = f_x$, $d_1(t), d_2(t)$ are bounded parameters perturbation terms. $g_1(X)$, $g_2(X)$, $b_2(X)$ are nonlinear functions as follows:

$$\begin{cases} g_1 = \dfrac{\xi_2\cos(\theta-\phi) - \xi_1}{M + m - m\cos^2(\theta-\phi)} \\ b_1 = \dfrac{1}{M + m - m\cos^2(\theta-\phi)} \\ g_2 = \dfrac{\xi_1\cos(\theta-\phi) - \xi_2\cos^2(\theta-\phi) - \xi_2 l(M + m - m\cos^2(\theta-\phi))}{l(M + m - m\cos^2(\theta-\phi))} \\ b_2 = -\dfrac{\cos(\theta-\phi)}{l(M + m - m\cos^2(\theta-\phi))} \end{cases}$$

where

$$\begin{aligned} \xi_1 = {} & -(M+m)h\ddot{\phi} + (M+m)(g+\ddot{y})\sin\phi - ml\dot{\theta}^2\sin(\theta-\phi) \\ & - (M+m)x\dot{\phi}^2 + m\ddot{l}\sin(\theta-\phi) + 2m\dot{l}\dot{\theta}\cos(\theta-\phi) \\ \xi_2 = {} & m\left(2\dot{l}\dot{\theta} + 2\dot{x}\dot{\phi}\sin(\theta-\phi) - x\dot{\phi}^2\cos(\theta-\phi) + x\ddot{\phi}\sin(\theta-\phi)\right. \\ & \left. - h\ddot{\phi}\cos(\theta-\phi) - h\dot{\phi}^2\sin(\theta-\phi) + (g+\ddot{y})\sin\theta\right) \end{aligned}$$

Assume that there exists positive constants g_{1M}, g_{2M}, d_{1M} and d_{2M} to ensure $g_1(X) \le g_{1M}$, $g_2(X) \le g_{2M}$ and $d_1(t) \le d_{1M}$, $d_2(t) \le d_{2M}$.

The entire system state is divided in to two sliding surfaces according to the general construction form of sliding surface: $s = \lambda e + \dot{e}$.

The target and real-time tracking positions of the trolley are defined as x_d and x, respectively. Plan the target swinging angle $\theta_d = 0$ and θ denotes the real-time swinging angle. Then error vector can be expressed as:

$$e = \begin{bmatrix} e_x & e_\theta \end{bmatrix}^T = \begin{bmatrix} x - x_d & \theta - \theta_d \end{bmatrix}^T \tag{11}$$

The first-layer of sliding surface can be defined as:

$$\begin{cases} s_1 = c_1 e_x + \dot{e}_x \\ s_2 = c_2 e_\theta + \dot{e}_\theta \end{cases} \tag{12}$$

where, c_1, c_2 are positive constants

The equivalent control terms u_{eq1} and u_{e2} on the sliding manifold of each subsystem can be calculated using equivalent control method as follows:

$$u_{eq1} = -\frac{g_1(X) + c_1 x_2 + d_1}{b_1} \tag{13}$$

$$u_{eq2} = -\frac{g_2(X) + c_2 x_4 + d_2}{b_2} \tag{14}$$

As a typical underactuated system, offshore crane system can hardly fulfill the position track of the trolley and loads anti-swing simultaneously with only one control input. For this reason, this paper ensures the synchronous combination control of such two objectives based on secondary sliding surface S by constructing the following second-layer sliding manifold:

$$S = \alpha s_1 + \beta s_2 \tag{15}$$

where, α is a positive constant, and β is a variable following the system states.

As for an underactuated system, the controller should ensure both the stability of actuated parts and the self-stability of underactuated parts. Therefore, to ensure each subsystem is on its own sliding surface, the total system control law must contain the control formula of each subsystem, which can be defined as:

$$\begin{aligned} u = u_{eq1} + u_{eq2} + u_{sw} = &-(\alpha b_1 - \beta b_2)^{-1} [\alpha(c_1 x_2 + g_1 + d_1) \\ &+ \beta(c_2 x_4 + g_2 + d_2) + \eta \operatorname{sgn}(S) + kS] \end{aligned} \tag{16}$$

where, u_{sw} is the switching control component when the system is at the reaching phase. η and k are positive control gains. K_1 is defined as:

$$K_1 = \sup_{t \ge 0} |u_{eq2} - u_{eq1}| \tag{17}$$

Each parameter of the controller needs to meet the following conditions:

$$\beta = \begin{cases} \beta_0 & s_1 s_2 > 0, \\ -\beta_0 & s_1 s_2 \le 0, \end{cases} \quad \beta_0 > 0; \tag{18}$$

$$\alpha > \frac{\beta_0 |b_2|}{b_1}, \beta_0 > 0; \tag{19}$$

$$\eta > |\beta||b_2| K_1 \tag{20}$$

Theorem 1: As for nonlinear system depicted in (10), sliding surfaces with double-layer structures are constructed based on (12) and (15). If controller is expressed in the form of (16) and its parameters satisfy (18) and (20), the second layer sliding surface S is stable, so is the first layer sliding surface s_1.

Proof:

The energy function based on Lyapunov theorem is built on the second layer sliding surface S. The Lyapunov function candidate is chosen as:

$$V(t) = \frac{1}{2} S^2 \tag{21}$$

The derivative of $V(t)$ in time is calculated as:

$$\begin{aligned} \dot{V}(t) &= S^T \dot{S} = S^T (\alpha \dot{s}_1 + \beta \dot{s}_2) \\ &= S^T [\alpha(c_1 x_2 + g_1 + b_1 u + d_1) \\ &\quad + \beta(c_2 x_4 + g_2 + b_2 u + d_2)] \\ &= -\eta \alpha s_1 - \eta \beta s_2 - (\alpha b_1 + \beta b_2) k S^2 \le 0 \end{aligned} \tag{22}$$

According to Lyapunov stability theorem, if $\dot{V} \le 0$, the system approaches asymptotic stability when $s = 0$ and so the second layer sliding surface S is stable.

Likewise, the Lyapunov energy function is built on the first layer sliding surface s_1 and can be denote as $V(t)_1 = \frac{1}{2} S_1^2$, whose time derivative is calculated as:

$$\begin{aligned}\dot{V}_1(t) &= s_1^T \dot{s}_1 = s_1^T \left(c_1 x_2 + g_1 + b_1 u + d_1\right) \\ &= \frac{b_1}{\alpha b_1 + \beta b_2}\left[b_2\left(u_{eq2} - u_{eq1}\right)\beta s_1 - \eta s_1\right] \\ &\quad - k^*\left(\alpha s_1^2 + \beta s_1 s_2\right)\end{aligned} \tag{23}$$

where, $k^* = b_1 k$ and $\alpha b_1 + \beta b_2 > 0$ can be guaranteed by (19). $\frac{b_1}{\alpha b_1 + \beta b_2} > 0$ because of $b_1 > 0$. So (23) can be simplified as:

$$\begin{aligned}\dot{V}_1 = s_1\dot{s}_1 &= \frac{b_1}{\alpha b_1 + \beta b_2}\left[b_2\left(u_{eq2} - u_{eq1}\right)\beta s_1 - \eta s_1\right] \\ &\quad - k^*\left(\alpha s_1^2 + \beta s_1 s_2\right) \\ &\le \frac{b_1}{\alpha b_1 + \beta b_2}\left(s_1 b_2 \beta K_1 - \eta s_1\right) - k^* \alpha s_1^2 \\ &= \frac{b_1}{\alpha b_1 + \beta b_2}\left(s_1 b_2 \beta K_1 - \eta s_1\right) - k^* \alpha s_1^2 \\ &\quad - k^* \beta s_1 s_2 \operatorname{sgn}\left(s_1 s_2\right)\end{aligned} \tag{24}$$

when $\eta > \beta b_2 K_1$ and β satisfies (18), $\dot{V}_1 < 0$. It follows that the first layer sliding surface s_1 is stable as well.

Theorem 2: As for nonlinear system described in (10), sliding surfaces with double-layers structures are constructed based on (12) and (15). The controller is in the form of (16). If s_1 and S are stable, then s_2 is stable as well.

Proof:

The first-order sliding mode surface s_1 is stable, indicating that s_1 has existence and reachability. With arbitrary initial condition s_{10}, there exists a time $t_1 (t_1 \in R^+)$ to ensure $\lim_{t \to t_1} s_1 = 0$, which means s_1 can converge to zero within finite time. Similarly, as for the S with arbitrary initial condition S_0, there exists a time $t_2 (t_2 \in R^+)$ to ensure $\lim_{t \to t_2} S = 0$. As a result, the sliding surface s_2 can be rewritten as:

$$\lim_{t \to T} s_2 = \lim_{t \to T} \frac{1}{\beta}\left(S - \alpha s_1\right) = 0 \tag{25}$$

Thus, the first-layer sliding surface s_2 is stable.

Remark 1: the proof of the stability of s_2 in theorem 2 is conservative, which means s_2 can converge to zero when any $t \ge T$. The conclusion is sufficient. But there is no explanation on whether s_2 can converge to zero when t < T. Actually, in addition to converging to zero with s_1 or S, s_2 may converge to zero with $S = \alpha s_1$ at a faster convergence rate than s_1 or S.

Remark 2: If the controller can ensure the stability of s_1 and S, it can control the sliding surface s_2 as well. It is thus evident that the presented control strategy can fulfill position track of the trolley and anti-swing of the payload simultaneously.

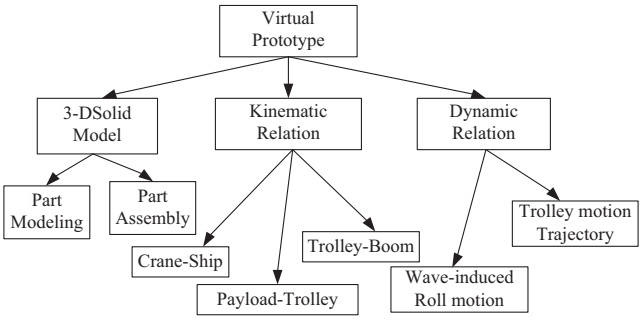

Fig. 5. Development process of OCC's virtual prototype.

Fig. 6. Multi-body dynamics mechanical model of OCC system.

IV. VIRTUAL PROTOTYPE SIMULATIONS

Since it is very time-consuming and difficult to build up an OCC and test it under real sea conditions, we utilize virtual prototype technology to testify the designed offshore container crane control system, which can help engineers to modify the mechanical design and improve the controller.

1. Multi-Body Dynamics Mechanical Model of OCC System

Considering the suspended rope as a flexible body, a rigid-flexible coupling multi-body dynamics model of OCC is constructed in ADAMS environment. The development process of OCC's virtual prototype is shown in Fig. 5.

Detailed steps are shown as follows: a 3D model of OCC system based on the actual size and shape is built using SOLIDWORKS and imported into ADAMS environment. Then, the parameters of the components such as mass, material property, moment of inertia, etc. must be defined. Next, by utilizing constraints, these parts are connected to each other. For example, the trolley is connected with the boom using translational joint. The crane gantry is mounted on the ship using fixed joint. The flexible cables are generated by Machinery/Cable module. The contact forces are added between winch and winded ropes (Dong, 2015). The ship is induced to roll and heave based on the wave disturbance function. The developed multi-body dynamics model of OCC system is shown in Fig. 6.

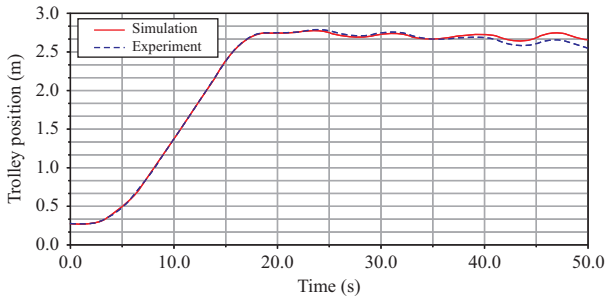

Fig. 7. The simulation and experimental results of trolley position.

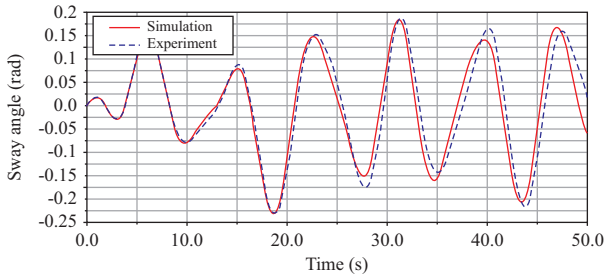

Fig. 8. The simulation and experimental results of sway angle.

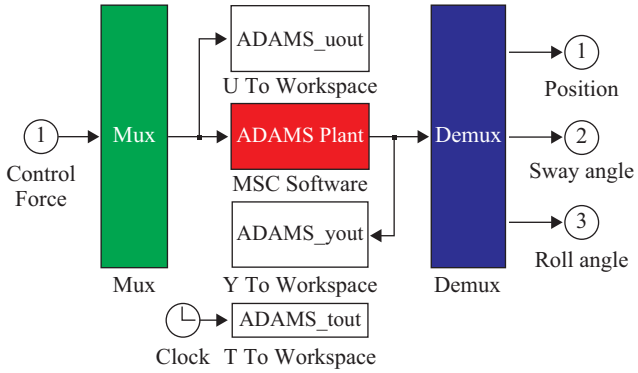

Fig. 9. The ADAMS module in MATLAB/SIMULINK.

The dynamic response of the crane without control is investigated. The motion of the trolley in x-axis direction is x = step (time, 0, 0, 18, 2.7). The parameters of virtual prototype are set as the experimental setup. The ship rolling motion is set as $\phi(t) = 0.01 \sin(0.5 \text{ time})$ rad. The simulation and experimental results are shown in Figs. 7 and 8, which illustrate the constructed model can imitate the real dynamics of OCC system. This model will be used in the subsequent simulation, verification and analysis of OCC control system.

2. Modeling of Control System

The control model of the proposed control strategy is built in Matlab/Simulink, which provides interface to ADAMS module shown in Fig. 9. The two software agents exchange signals by transferring state variables in a closed loop shown in Fig. 10.

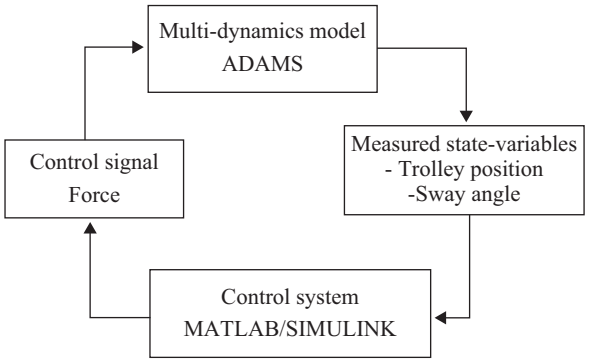

Fig. 10. The communication of ADAMS and MATLAB/SIMULINK.

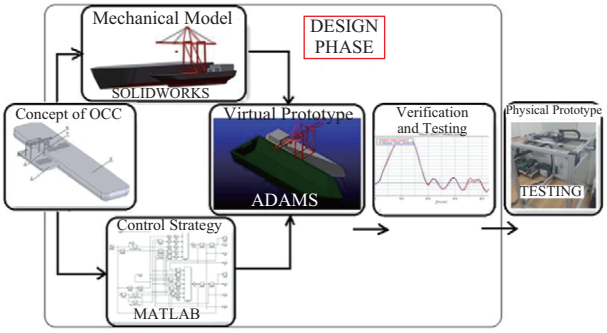

Fig. 11. The mechatronics virtual prototype.

Combine the ADAMS mechanical model with controller based on MATLAB/Simulink, the mechatronics virtual prototype is established, as illustrated in Fig. 11.

3. Co-Simulation Results

Co-simulation results of the virtual prototype are collected to illustrate the performance of the proposed controller. In order to demonstrate increased performance of the proposed controller versus conventional controller, the simulation results of the conventional PID controller are also provided.

According to the real OCC, the parameters of the system are chosen as: $h = 48$ m, $M = 2.0 \times 10^4$ kg, $l = 15$ m, $x_d = 36$ m, $\phi(t) = 0.007 \sin(1.25\ t)$ rad (Sea State 3), $\phi(t) = 0.0165 \sin(0.924\ t)$ rad (Sea State 4) and $\phi(t) = 0.0286 \sin(0.714\ t)$ rad (Sea State 5).

(1) Co-simulation results of PID controller

In order to control the position and sway simultaneously, the double-PID controllers are selected including position PID and sway PID. The controller parameters are sufficiently tuned to obtain the best performance, which yields the following values:

$$P_k = 2500,\ P_i = 100,\ P_d = 18000 \text{ for position PID.}$$

$$P_{ks} = 500,\ P_{is} = 20,\ P_{ds} = 700 \text{ for sway PID.}$$

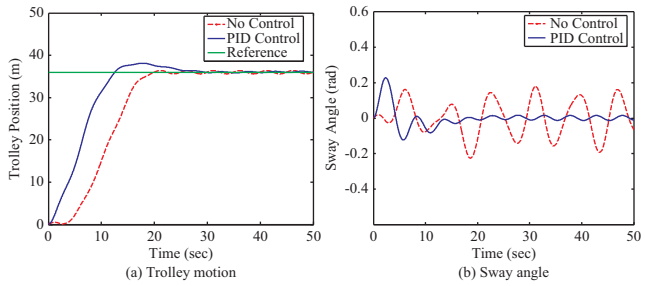

Fig. 12. The tracking and anti-sway results of PID controller with f_{roll} = 1.25, δ_{roll} = 0.007 (sea state 3).

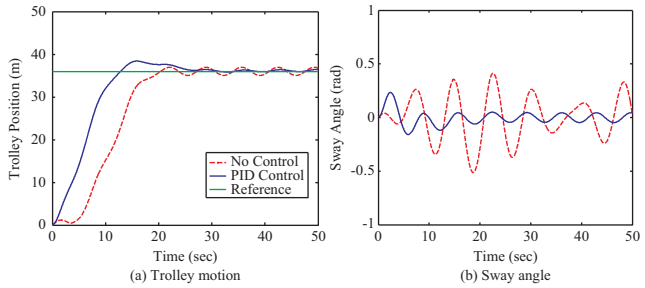

Fig. 13. The tracking and anti-sway results of PID controller with f_{roll} = 0.924, δ_{roll} = 0.0165 (sea state 4).

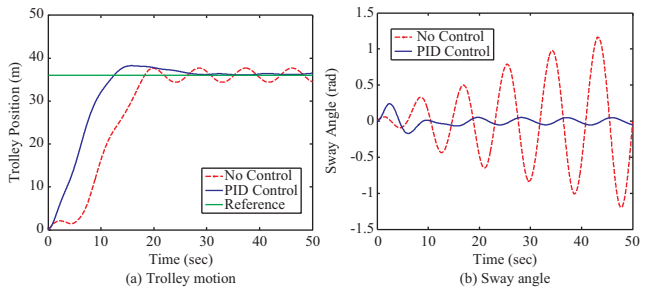

Fig. 14. The tracking and anti-sway results of PID controller with f_{roll} = 0.714, δ_{roll} = 0.0286 (sea state 5).

f_{roll} and δ_{roll} denote roll frequency and amplitude of ϕ. The tracking and anti-sway results are depicted in Figs. 12-14.

(2) Co-simulation results of the proposed controller

The optimal parameters of the proposed SOSM controller yield the following values:

$$c_1 = 0.8,\ c_2 = 0.4,\ \alpha = 3.2,$$

$$\beta = 0.4,\ \eta = 0.53,\ k = 2$$

The tracking and anti-sway results are shown in Figs. 15-17.

The control goals of OCC system include tracking the trolley position quickly and suppressing the payload swing. The desired specifications are required as follows:

Settling time $\leqslant$ 15 s; Overshoot $\leqslant$ 2 %; Steady state error $\leqslant$ ±0.05 m; Residual swing $\leqslant$ ±0.05 rad.

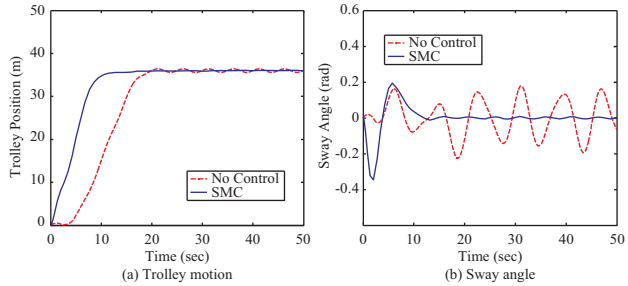

Fig. 15. The tracking and anti-sway results of the proposed controller with f_{roll} = 1.25, δ_{roll} = 0.007 (sea state 3).

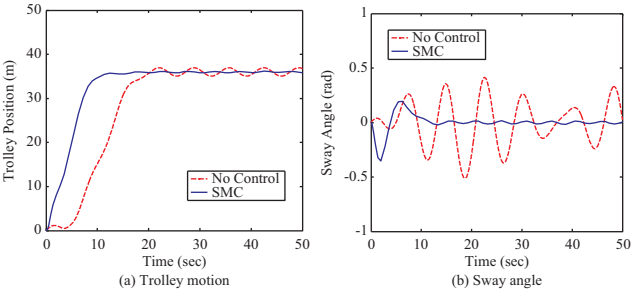

Fig. 16. The tracking and anti-sway results of proposed controller with f_{roll} = 0.924, δ_{roll} = 0.0165 (sea state 4).

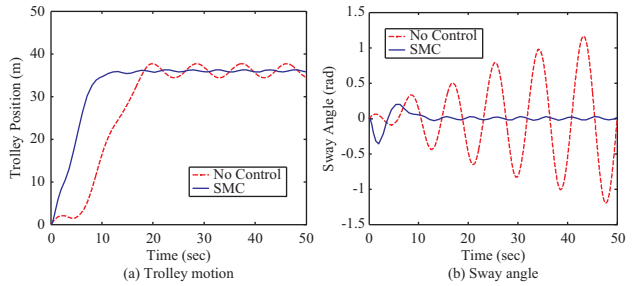

Fig. 17. The tracking and anti-sway results of proposed controller with f_{roll} = 0.714, δ_{roll} = 0.0286 (sea state 5).

According to the Figs. 12-17, the relevant data statistics are listed in the Tables 1 and 2 to evaluate the control performance. The co-simulation results demonstrate that conventional PID controller's settling time is much longer than the required time and the residual sway angle also can't meet the requirement of control goal. For the proposed SOSM controller, overshoot = 0.74%-0.87%, settling time = 10.9-12.1 second and steady state error is 0.02-0.04 m upon sea state 3 & 4, which can satisfy the control goal perfectly. But due to the ship moves sharply on the sea state 5, the trolley can't achieve accurate positioning with the steady state error of 0.11 m.

In summary, for the novel OCC system, because of the complexity of marine environment, the conventional PID control method no longer meet the control goals. The proposed anti-sway tracking controller has a good performance and strong robustness. It can track the desired position quickly and accurately with rather small residual sway angle upon sea state 3 and 4.

Table 1. The comparison of the trolley position response.

external disturbance	Control method	Settling time (s)	Overshoot (%)	steady-state error (m)
Sea State 3	none	/	/	0.20
	PID	23.6	4.92	0.12
	SOSM	10.9	0.74	0.02
Sea State 4	none	/	/	0.40
	PID	24.5	5.23	0.15
	SOSM	11.3	0.81	0.04
Sea State 5	none	/	/	1.21
	PID	25.2	5.60	0.38
	SOSM	12.1	0.87	0.11

Table 2. The comparison of the payload sway angle response.

external disturbance	Control method	Settling time (s)	residual sway angle (rad)
Sea State 3	none	/	/
	PID	18.6	0.030
	SOSM	12.0	0.008
Sea State 4	none	/	/
	PID	20.8	0.050
	SOSM	12.3	0.013
Sea State 5	none	/	/
	PID	24.4	0.058
	SOSM	13.1	0.025

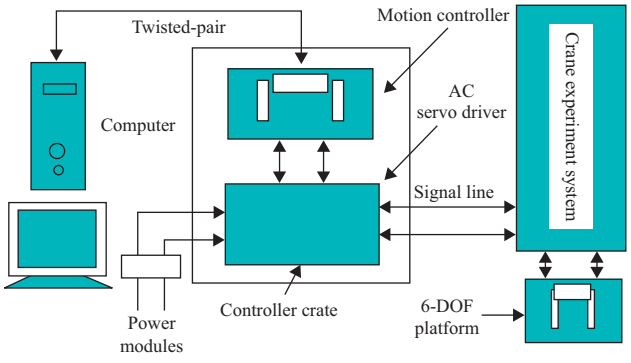

Fig. 18. Structure of the experimental test bed.

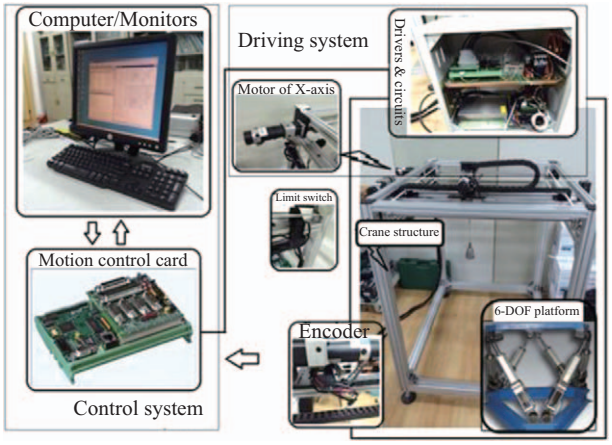

Fig. 19. Experimental system.

V. EXPERIMENTAL RESULTS

After sufficient simulation tests, much effort has been put to perform experiments to further evaluate the performance of the proposed control strategy.

Since it is hard to build an offshore container crane attached in a mobile harbor with disturbance from currents and waves, an experimental setup is established as illustrated in Fig.18.

The test bed includes crane structure, 6-DOF motion platform, angular and displacement sensors (encoders), driving system and controller crate shown in Fig. 19. The 6-DOF platform can imitate the roll motion of the ship. The upper computer utilizes Matlab/Simulink RTWT (Real Time Windows Target) as real-time control platform. The DMC-1842 motion control card is chosen to programme the upper computer's output signal, whose functional block diagram is plotted in Fig. 20.

The experimental system parameters are set to be:

$$h = 2.5 \text{ m}, M = 16 \text{ kg}, m = 4 \text{ kg}, l = 0.7 \text{ m}, x_d = 0.5 \text{ m}.$$

For the experiments, the parameters and gains of SOSM controller are carefully determined as follows:

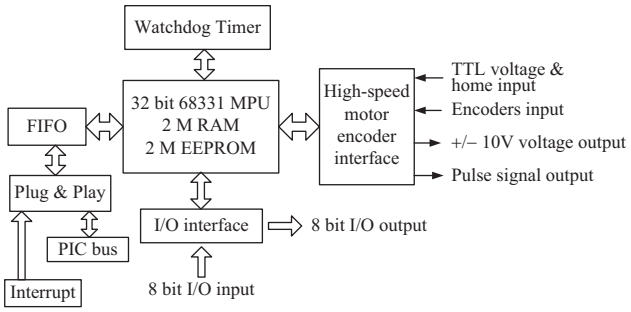

Fig. 20. Functional block diagram of motion control card.

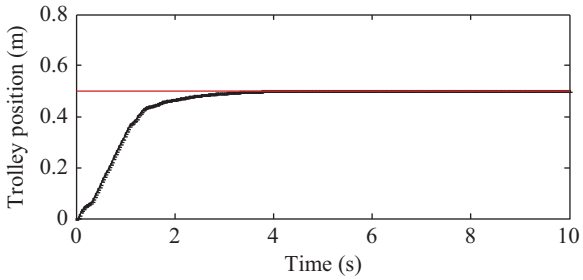

Fig. 21. Results of Experiment 1: trolley's position.

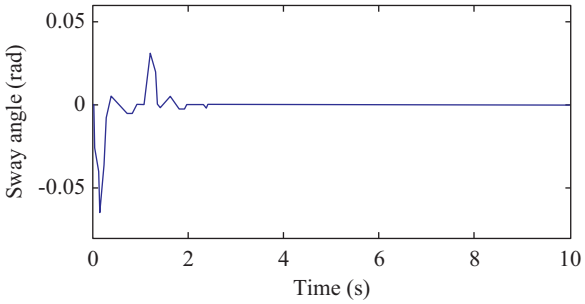

Fig. 22. Results of Experiment 1: payload's sway angle.

$$c_1 = 1, c_2 = 14, \alpha = 3.28, \beta = 1, k = 22, \eta = 1$$

To fully investigate the performance of the proposed track position & anti-sway control strategy, two sets of experiments are implemented to evaluate the controller's tracking performance and the sway suppression capacity, respectively.

Experiment 1: Proposed Controller without Ship Motion

The experimental results for the proposed control algorithm are provided in Figs. 21 and 22 in experiment of the ship is stationary ($\phi = 0$). we can find that the sway angle is eliminated remarkably within 2 seconds before the trolley reach its desired position.

Experiment 2: Proposed Controller with the Ship Roll Motion

The roll motion of the ship used for the experiment verifications is depicted in the Fig. 23.

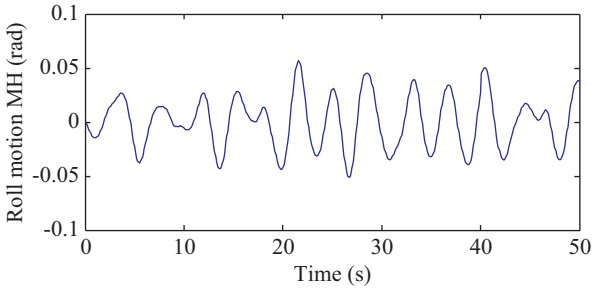

Fig. 23. The rolling angle.

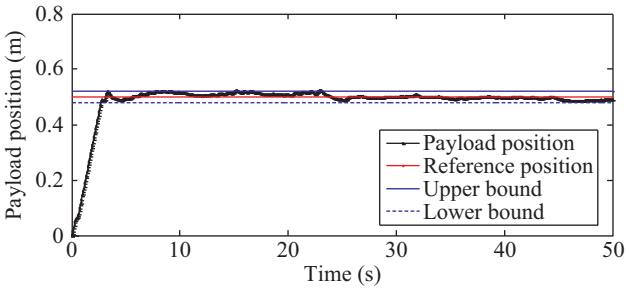

Fig. 24. Results of Experiment 2: trolley's position.

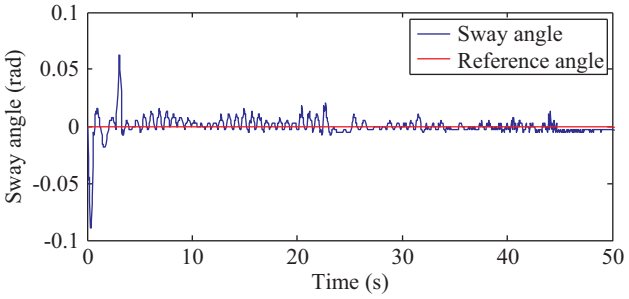

Fig. 25. Results of Experiment 2: payload's sway angle.

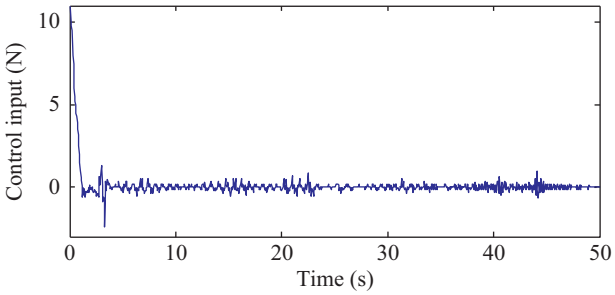

Fig. 26. Results of Experiment 2: control force.

Figs. 24-26 illustrate the control performance of the designed control strategy with the existent motion of ship. Fig. 24 shows that the trolley can track the goal position quickly and the position error stays within an acceptable motion region [-0.02 m, 0.02 m]. It can be found in Fig. 25 that the payload

maintains small residual sway angle less than 0.02 rad, which can satisfy the control objective remarkably.

VI. COCLUSION

In this paper, we have addressed the problem of payload sway suppression and trolley position track for OCC system with disturbances of ship motions and parameters perturbation. By utilizing Euler-Lagrange equations, the mathematical model of OCC system is derived comprehensively and a SOSM control strategy is presented to achieve the control goal. A virtual prototype of OCC is established and extensive simulation results show a good cancellation of the track error and residual sway upon sea state 3 and 4, but not so satisfying on sea state 5. Experimental results are provided to examine its practical control performance. The designed method is also applicable to other types of cranes with convenient modification (including gantry cranes and tower cranes) and can be used for reference to control other underactuated mechatronic systems as well.

ACKNOWLEGDEMENTS

This research was supported by the National Natural Science Foundation of China (No. 51505277).

REFERENCES

Almutairi, N. B. and M. Zribi (2009). Sliding mode control of a three-dimensional overhead crane. Journal of Vibration and Control 15(11), 1679-1730.

Baird, A. J. and D. Rother (2013). Technical and Economic Evaluation of the Floating Container Storage and Transhipment Terminal (Fcstt), Transportation Research Part C-Emerging Technologies 30, 178-92.

Centre AS (OSC): A Flexible Framework for Alternative Maritime Crane Control Algorithms. IEEE Journal of Oceanic Engineering 41(2), 450-461.

Chang, C. Y. (2007). Adaptive fuzzy controller of the overhead cranes with nonlinear disturbance. IEEE Transactions on Industrial Informatics 3(2), 164-172.

Cha, J. H., M. I. Roh and K. Y. Lee (2010). Dynamic response simulation of a heavy cargo suspended by a floating crane based on multibody system dynamics. Ocean Engineering 37, 1273-1291.

Chin, C. M., A. H. Nayfeh and D.T. Mook (2001). Dynamics and control of ship-mounted cranes. Journal of Vibration and Control 7(6), 891-904.

Garrido, S., M. Abderrahim and A. Gimenez (2008). Anti-swinging input shaping control of an automatic construction crane. IEEE Transactions on Automation Science and Engineering 5(3), 549-557.

Do, K. D., Z. P. Jiang and J. Pan (2002). Universal controllers for stabilization and tracking of underactuated ships. Systems & Control Letters 47(4), 299-317.

Dong, D. S., Y. G. Sun, L. Liu and H. Y. Qiang (2015). Simulation study on dynamic characters of floating crane based on virtual prototype technology. Mechanical Science and Technology for Aerospace Engineering 34(3), 393-397. (In Chinese)

Ham, S. H., M. I. Roh, H. Lee and S. Ha (2015). Multibody dynamic analysis of a heavy load suspended by a floating crane with constraint-based wire rope. Ocean Engineering 109, 145-160.

Henry, R. J., Z. N. Masoud, A. H. Nayfeh and D. T. Mook (2001) Cargo pendulation reduction on ship-mounted cranes via boom-luff angle actuation. Journal of Vibration and Control 7(8), 1253-1264.

Hilhorst, G., G. Pipeleers and W. Michiels (2015). Reduced-Order H-2/H-infinity Control of discre-time lpv systems with experimental validation on an overhead crane test setup. Proceedings of the American Control Conference Chicago, 125-130.

Hong, K. S. and Q. H. Ngo (2009). Crane and ship loading thereof. Korean Patent. 10-2009-0126946.

Ismail, R. M. T. R., N. D. That and Q. P. Ha (2015). Modelling and robust trajectory following for offshore container crane systems. Automation in Construction 59, 179-187.

Jang, I. G., K. S. Kim and B. M. Kwak (2014). Conceptual and basic designs of the mobile harbor crane based on topology and shape optimization. Structural and Multidisciplinary Optimization 50, 505-15.

Jin, J. and X. H. Zhang (2016). Multi AGV scheduling problem in automated container terminal. Journal of Marine Science and Technology-Taiwan 24(1), 32-38.

Jonghoe, K. and R. M. James (2012). Offshore port service concepts: Classification and economic feasibility. Flexible Services and Manufacturing Journal 24, 214-45.

Kuchler, S., T. Mahl, J. Neupert, K. Schneider and O. Sawodny (2011). Active control for an offshore crane using prediction of the vessel's motion. IEEE-ASME Transactions on Mechatronics 16(2), 297-309.

Le, A. T., S. G. Lee and C. N. Luong (2015). Robust controls for ship-mounted container cranes with viscoelastic foundation and flexible hoisting cable. Proceedings of the Institution of Mechanical Engineers Part I-Journal of Systems and Control Engineering 229(7), 662-674.

Li, Y. M., S. C. Tong and T. Li (2015) Observer-based adaptive fuzzy tracking control of MIMO stochastic nonlinear systems with unknown control direction and unknown dead-zones. IEEE Transactions on Fuzzy Systems 23(4), 1228-1241.

Ngo, Q. H. and K. S. Hong (2012). Sliding-mode antisway control of an offshore container crane. IEEE-ASME Transactions on Mechatronics 17(2), 201-209.

Oscar, A. S., C. S. Pedro and M. C. Rafael (2015). The impact on port competition of the integration of port and inland transport services. Transportation Research Part B-Methodological 80, 291-302.

Park, H. S. and N. T. Le (2012). Modeling and Controlling the Mobile Harbour Crane System with Virtual Prototyping Technology. International Journal of Control Automation and Systems 10(6), 1204-1214.

Saeidi, H., M. Naraghi and A. A. Raie (2013). A neural network self tuner based on input shapers behavior for anti sway system of gantry cranes. Journal of Vibration and Control 19(13), 1936-1949.

Sanfilippo, F., L. I. Hatledal and A. Styve (2016). Integrated flexible maritime crane architecture for the offshore simulation centre AS (OSC): A Flexible framework for alternative maritime crane control algorithms. IEEE Journal of Oceanic Engineering 41(2), 450-461.

Serrano, M. E., G. J. E. Scaglia and S. A. Godoy (2014). Trajectory Tracking of underactuated surface vessels: a linear algebra approach. IEEE Transactions on Control Systems Technology 22(3), 1103-1111.

Skaare, B. and O. Egeland (2006). Parallel force/position crane control in marine operations. IEEE Journal of Oceanic Engineering 31(3), 599-613.

Sun, Y. G., W. L. Li, S. D. Dong, X. Mei and H. Y. Qiang (2015). Dynamics analysis and active control of a floating crane. Tehnicki Vjesnik-Technical Gazette 22(6), 1383-1391.

Sun, Y., H. Qiang, X. Mei and Y. Teng (2017). Modified repetitive learning control with unidirectional control input for uncertain nonlinear systems, Neural Computing and Applications, 1-10.

Terashima, K., Y. Shen and K. Yano (2007). Modeling and optimal control of a rotary crane using the straight transfer transformation method, Control Engineering Practice 15(9), 1179-1192.

Wang, Y. (2013). Research and design of an anti-swing mechanism for a ship-borne crane. Ship Science and Technology 35(7), 105-108. (In Chinese)

Woodacre, J. K., Bauer, R. J., Irani, R. A.(2015). A review of vertical motion heave compensation systems. Ocean Engineering 104, 140-154.

Wu, T. S., M. Karkoub, W. S. Yu and C. T. Chen (2016). Anti-sway tracking control of tower cranes with delayed uncertainty using a robust adaptive fuzzy control. Fuzzy Sets and Systems 290, 118-137.